An analytical investigation: Effect of solar wind on lunar photoelectron sheath

S. K. Mishra, and Shikha Misra

Citation: Physics of Plasmas **25**, 023702 (2018);
View online: https://doi.org/10.1063/1.5021260
View Table of Contents: http://aip.scitation.org/toc/php/25/2
Published by the American Institute of Physics

An analytical investigation: Effect of solar wind on lunar photoelectron sheath

S. K. Mishra[1,a)] and Shikha Misra[2,3]
[1]*Extreme Light Infrastructure-Attosecond Light Pulse Source (ELI-ALPS), Szeged 6720, Hungary*
[2]*Rakesh P. G. College, Pilani 333031, India*
[3]*F-32, CSIR-CEERI Col. Pilani 333031, India*

(Received 2 January 2018; accepted 18 January 2018; published online 5 February 2018)

The formation of a photoelectron sheath over the lunar surface and subsequent dust levitation, under the influence of solar wind plasma and continuous solar radiation, has been analytically investigated. The photoelectron sheath characteristics have been evaluated using the Poisson equation configured with population density contributions from half Fermi-Dirac distribution of the photoemitted electrons and simplified Maxwellian statistics of solar wind plasma; as a consequence, altitude profiles for electric potential, electric field, and population density within the photoelectron sheath have been derived. The expression for the accretion rate of sheath electrons over the levitated spherical particles using anisotropic photoelectron flux has been derived, which has been further utilized to characterize the charging of levitating fine particles in the lunar sheath along with other constituent photoemission and solar wind fluxes. This estimate of particle charge has been further manifested with lunar sheath characteristics to evaluate the altitude profile of the particle size exhibiting levitation. The inclusion of solar wind flux into analysis is noticed to reduce the sheath span and altitude of the particle levitation; the dependence of the sheath structure and particle levitation on the solar wind plasma parameters has been discussed and graphically presented. *Published by AIP Publishing.* https://doi.org/10.1063/1.5021260

I. INTRODUCTION

The observation of lunar horizon glow and streamers over the moon surface by Apollo lunar missions[1] was the first signature of the dusty environment on the moon where sunlight scattering is primarily caused by charged dust particles originating from the lunar surface.[2] In the absence of the atmosphere, the frequent impact of debris/asteroids over the lunar surface generates fine dust exhibiting a broad size distribution.[3] The moon surface and fine particles get charged under direct exposure of solar radiation and wind plasma, giving rise to the phenomena of sheath formation and dust levitation. The direct observations[1–6] of dust over the lunar surface via Surveyor spacecraft and by the Apollo-17 orbiting command module and its analysis led to an intuitive understanding and theoretical development of electrostatic dust levitation.[3] In this context, multiple experimental/theoretical/simulation investigations have been performed to interpret the phenomenon of sheath formation and particle levitation;[7–17] for instance, recent work[15] predicts the fine nanometer sized (∼10 nm) particles' levitation up to ∼10s of meters while the sub-micron (∼100–250) nm grains can float up to an altitude of (∼1–100) cm.

A significant analysis interpreting the photoelectron sheath over the lunar surface was presented by Nitter *et al.*,[18] where the incoming and outgoing photoelectrons were consistently taken into account to evaluate the sheath structure; however, an oversimplified isotropic Maxwellian distribution of emitted photoelectrons was considered. In order to include the anisotropic feature of the photoemitted electrons in evaluating incoming/outgoing flux over levitated dust particles, later Nitter's[18] analysis was modified by including arbitrary half Maxwellian distribution[12–17] of the photoemitted electrons; however, this is still a simplified assumption of the photoelectron distribution which essentially should be half Fermi-Dirac energy distribution.[19,20] In a recent work, the analysis has been further re-formulated by Sodha and Mishra[21] by including the adequate half Fermi-Dirac statistics of photoemitted electrons along with appropriate expressions for photoemission flux; the sheath features over the lunar surface are shown to be significantly different from those predicted by half Maxwellian statistics. The consideration of Maxwellian distribution[21] of the surface electrons predicts a smaller photoemission rate with respect to FD statistics, which ultimately reduces the lunar surface potential and the subsequent population density in the sheath; this results in a larger sheath, weaker potential decay, and smaller electric field in the sheath, which also infers a smaller altitude of the particle levitation. In their analysis,[21] the expressions for the electron accretion flux over levitated dust particles have been derived considering the anisotropic flux in the photoelectron sheath, which has been further used in evaluating the size distribution of the levitating dust particles; the analysis was performed for the dominant extreme ultraviolet (EUV) Lyman-α radiation. Later this analysis is extended to a continuous solar spectrum in deriving an asymmetric sheath formation around spherical objects orbiting in near-earth space.[22] Although these earlier analyses[21–23] put forward a significant physical understanding of the sheath formation, the contribution from solar wind plasma in

a)E-mail: nishfeb@gmail.com

photoelectron sheath formation has been ignored; some of the recent simulation studies[24–26] highlight the role of solar wind plasma in the lunar photoelectron sheath and subsequent dust transport. This feature has been analytically addressed in this work.

In this work, we take account of our recent analysis[21] to formulate the sheath formation and particle levitation over the moon surface irradiated by a continuous solar spectrum and solar wind flux. Using the Fowlers approach of photoemission of electrons (from the moon surface and dust particles), anisotropic half Fermi-Dirac statistics for the photoemitted electrons, simplified Maxwellian distribution for solar wind plasma, continuous solar spectrum (black body radiation at 5800 K[27] plus Lyman-α radiation[28]), and balance of charge (over the moon surface and levitated dust particles) along with the Poisson equation, the steady state altitude dependence of the electric potential, electric field, population density, and particle size on the lunar photoelectron sheath has been investigated.

This manuscript has been organized as follows: The formulation for the sheath structure over the lunar surface composed of photoelectron and solar wind plasma population has been derived in Sec. II; the computational scheme and numerical results/discussion for the photoelectron sheath over the lunar surface have been presented in Sec. III. The levitation of dust particles along with the evaluation of constituent photoemission flux, anisotropic flux in photoelectron sheath, and solar wind flux has been discussed in Sec. IV; based on this analysis, the numerical results for the dust charging and their levitation within lunar photoelectron sheath have been presented in Sec. V. A summary of the outcome in Sec. VI concludes this paper.

II. SHEATH MODEL

The sheath formation in the proximity of the moon surface is caused by dynamic equilibrium between the photoemission flux and return (accretion) current over its surface, maintaining it at positive potential. Analytically, the sheath characteristics may be modelled by evaluating the net plasma (electron/ion) population density in the space over the lunar surface and utilizing it in solving the Poisson equation. The continuous solar wind and solar radiation (causing photoemission) incident over lunar surface may be considered as a principal source for the plasma population. In order to analyze the sheath structure, we follow the approach adopted in Ref. 21 and modify the analysis by including the additional effects of solar wind plasma and white light (i.e., continuous solar radiation spectrum) in determining the effective plasma density in the space over the lunar surface. Concerning the large curvature of the moon, its surface may be considered as the horizontal (planar) surface for all the practical realization. Further, due to the large distance between the sun and moon, the lunar surface may be considered to be uniformly irradiated via solar wind and solar spectrum. With these simplifications, we next evaluate the contribution from solar radiation and solar wind in determining the plasma population density over the moon surface.

A. Photoelectron population

The solar radiation falling on the lunar surface (regolith) includes the continuous solar spectrum[27] in addition to a dominant Lyman-α ($\lambda \sim 121.57$ nm) spectrum in the EUV (extreme ultraviolet) regime;[28] the entire range of solar radiation is considered to cause photoemission of the electrons from the lunar regolith (and levitated particles). The continuous radiation from the sun may adequately be approximated as a black body radiating at temperature $T_s \sim 5800$ K. The net photon flux associated with the solar radiation reaching (normally) the sunlit surface of the moon and available for photoemission may approximately be expressed as[27–29]

$$\Lambda_{inc} = (\Lambda_{cr} + \Lambda_{L\alpha}) = \left[\int_{\varepsilon_{\nu 0}}^{\varepsilon_{\nu m}} d\Lambda_{cr} + \Lambda_{L\alpha}\right] = \left[\left(\frac{4\pi}{c^2}\right)\left(\frac{e}{300h}\right)^3\left(\frac{r_s^2}{r_d^2}\right)\int_{\varepsilon_{\nu 0}}^{\varepsilon_{\nu m}} E_\nu^2[\exp(E_\nu/kT_s) - 1]^{-1} \times dE_\nu + \Lambda_{L\alpha}\right], \quad (1)$$

where $r_s (\approx 6.96 \times 10^{10}\,\text{cm})$ is the radius of the radiating surface of the sun, $r_d (\approx 1.45 \times 10^{13}\,\text{cm})$ refers to the mean distance between the sun and moon, T_s is the temperature of the radiating sun, $E_{\nu 0} (= \phi + V)$ and $E_{\nu m}$ are the lower and upper limits of the useful solar radiation spectrum, ϕ and V are the work function and surface potential of the moon/dust surface materials, $\Lambda_{L\alpha} (= 3 \times 10^{11}\,\text{cm}^{-2}\,\text{s}^{-1})$ corresponds to the photon flux associated with Lyman-α radiation,[28] and e, k, and h are the Planck constant, Boltzmann constant, and electronic charge; here, E_ν is expressed in eV.

Following the approach adopted in Ref. 21, the momentum distribution of the outgoing photoelectrons due to the incident solar radiation, emitted per unit area per unit time from the lunar plane just outside the surface ($x = 0$) having a potential V_o (lunar surface), can be written as

$$d^2 n_{ph}(\upsilon_o) = \left[\int_{\varepsilon_{\nu 0}}^{\varepsilon_{\nu m}} \left(\frac{\chi(\varepsilon_\nu)}{\Phi(\varsigma_r)}\right)[F_D(\varepsilon_x + \varepsilon_t - \varsigma_r)d\varepsilon_x d\varepsilon_t]d\Lambda_{cr} + \left(\frac{\chi(\varepsilon_{L\alpha})}{\Phi(\varsigma_{r,L\alpha})}\right)\Lambda_{L\alpha} F_D(\varepsilon_x + \varepsilon_t - \varsigma_{r,L\alpha})d\varepsilon_x d\varepsilon_t\right], \quad (2)$$

where $\chi(\varepsilon_\nu)$ is the photoelectric efficiency of the surface material, $\varsigma_r = (\varepsilon_\nu - \varphi_r)$, $\varsigma_{r,L\alpha} = (\varepsilon_{L\alpha} - \varphi_r)$, $\varphi_r = (e\phi_r/kT_o)$, $\varepsilon_\nu = E_\nu/kT_o$, $\varepsilon_{L\alpha} = E_{L\alpha}/kT_o$, $\varepsilon_{\nu m} = E_{\nu m}/kT_o$, $\varepsilon_{\nu 0} = E_{\nu 0}/kT_o$, $\upsilon_o = -eV_o/kT_o$, $F_D(\eta) = (1 + \exp\eta)^{-1}$ refers to the Fermi-Dirac distribution,[30] ϕ_r refers to the work function of the lunar regolith, T_o refers to the temperature of the emitting surface, ε_x and ε_t are the normal and parallel components of the photoelectron energy (normalized with kT_o), and $\Phi(\varsigma) = \int_0^{\exp\varsigma} \Omega^{-1} \ln(1 + \Omega)d\Omega$. Considering the spectral dependence of the photoelectric yield of the emitting surface, Draine's formulation[31] describing its spectral dependence has been taken into account. Algebraically, this relation can be expressed as $\chi(\varepsilon_\nu) = \chi_0[1 - (\varphi/\varepsilon_\nu)]$, where χ_0 is the maximum photoelectric yield.

This electron flux traverses in space normal to the lunar surface and gives rise to electron density population. Consider a virtual plane parallel to the horizontal lunar surface (at finite x) at potential V (υ in normalized units). Following the approach similar to Ref. 21, the momentum distribution in reference to the virtual surface (at surface potential V) corresponding to Eq. (2) can be written as

$$d^2n_{ph}(\upsilon)=\left[\int_{\varepsilon_{\nu 0}}^{\varepsilon_{\nu m}}\left(\frac{\chi(\varepsilon_\nu)}{\Phi(\varsigma_r)}\right)[F_D(\varepsilon_x+\varepsilon_t-\varsigma_r-\upsilon_o+\upsilon)d\varepsilon_x d\varepsilon_t]d\Lambda_{cr}+\left(\frac{\chi(\varepsilon_{L\alpha})}{\Phi(\varsigma_{r,L\alpha})}\right)\Lambda_{L\alpha}F_D(\varepsilon_x+\varepsilon_t-\varsigma_{r,L\alpha}-\upsilon_o+\upsilon)d\varepsilon_x d\varepsilon_t\right]. \tag{3}$$

The emission flux across the virtual plane (at potential V) may be determined by integrating the above expression [Eq. (3)] over the parallel and normal energy components with appropriate limits. The net electron flux available to cross the virtual plane having normal energy ε_x and $\varepsilon_x+d\varepsilon_x$ may be written by integrating Eq. (3) over $\varepsilon_t\in(0,\infty)$ as

$$dn_{ph}(\upsilon)=\left[\int_{\varepsilon_{\nu 0}}^{\varepsilon_{\nu m}}\left(\frac{\chi(\varepsilon_\nu)}{\Phi(\varsigma_r)}\right)ln[1+\exp[-(\varepsilon_x-\varsigma_r-\upsilon_o+\upsilon)]]\times d\varepsilon_x d\Lambda_{cr}+\left(\frac{\chi(\varepsilon_{L\alpha})}{\Phi(\varsigma_{r,L\alpha})}\right)\Lambda_{L\alpha}ln\times\left[1+\exp\left[-(\varepsilon_x-\varsigma_{r,L\alpha}-\upsilon_o+\upsilon)\right]\right]d\varepsilon_x\right]. \tag{4}$$

The outward photoelectron flux through the virtual plane may be obtained by integrating Eq. (4) over normal energy space $\varepsilon_x\in(0,\infty)$ and may be expressed as

$$n_{pho}(\upsilon)=\left[\int_{\varepsilon_{\nu 0}}^{\varepsilon_{\nu m}}\left[\frac{\Phi(\upsilon_o-\upsilon+\varsigma_r)}{\Phi(\varsigma_r)}\right]\chi(\varepsilon_\nu)d\Lambda_{cr}+\left[\frac{\Phi(\upsilon_o-\upsilon+\varsigma_{r,L\alpha})}{\Phi(\varsigma_{r,L\alpha})}\right]\chi(\varepsilon_{L\alpha})\Lambda_{L\alpha}\right]. \tag{5}$$

The electrons having the normal energy $\varepsilon_x<-\upsilon(=eV/kT_o)$ return back to the virtual plane and hence the inward electron flux may be written by integrating Eq. (4) over normal energy space $\varepsilon_x\in(0,-\upsilon)$ as

$$n_{phi}(\upsilon)=\left[\int_{\varepsilon_{\nu 0}}^{\varepsilon_{\nu m}}\left[\frac{\Phi(\upsilon_o-\upsilon+\varsigma_r)-\Phi(\upsilon_o+\varsigma_r)}{\Phi(\varsigma_r)}\right]\chi(\varepsilon_\nu)d\Lambda_{cr}+\left[\frac{\Phi(\upsilon_o-\upsilon+\varsigma_{L\alpha})-\Phi(\upsilon_o+\varsigma_{r,L\alpha})}{\Phi(\varsigma_{r,L\alpha})}\right]\chi(\varepsilon_{L\alpha})\Lambda_{L\alpha}\right]. \tag{6}$$

The net electron flux coming out from the virtual plane may be expressed as

$$n_{ph}(\upsilon)=\left[n_{pho}(\upsilon)-n_{phi}(\upsilon)\right]=\left[\int_{\varepsilon_{\nu 0}}^{\varepsilon_{\nu m}}\left[\frac{\Phi(\upsilon_o+\varsigma_r)}{\Phi(\varsigma_r)}\right]\chi(\varepsilon_\nu)d\Lambda_{cr}+\left[\frac{\Phi(\upsilon_o+\varsigma_{r,L\alpha})}{\Phi(\varsigma_{r,L\alpha})}\right]\chi(\varepsilon_{L\alpha})\Lambda_{L\alpha}\right]. \tag{7}$$

From Eq. (7), it is evident that in the steady state, the net flux of photoemitted electrons across all the virtual planes (all υ's/x's) over the lunar surface is independent of the potential of the virtual surface (υ) and is equivalent to the flux from the regolith surface (at $x=0$); it should be stated that the net flux is a significant function of the steady state lunar surface potential (υ_o). Using Eq. (4), the electron densities associated with the outward and inward fluxes and hence the net electron density due to photoemission through virtual plane can be written as

$$n_{peo}(\upsilon)=(m/2kT_o)^{1/2}\int_0^\infty \varepsilon_x^{-1/2}dn_{ph}(\upsilon), \tag{8}$$

$$n_{pei}(\upsilon)=(m/2kT_o)^{1/2}\int_0^{-\upsilon} \varepsilon_x^{-1/2}dn_{ph}(\upsilon), \tag{9}$$

and

$$n_{pe}(\upsilon)=\left[n_{epo}(\upsilon)+n_{epo}(\upsilon)\right]=(m/2kT_o)^{1/2}\left[\int_0^\infty \varepsilon_x^{-1/2}dn_{ph}(\upsilon)+\int_0^{-\upsilon} \varepsilon_x^{-1/2}dn_{ph}(\upsilon)\right]. \tag{10}$$

Equation (10) infers the electron density at any virtual plane at vertical altitude (x) due to photoemission as a function of steady state surface potential of lunar regolith and the temperature of the emitting surface (T_o). Next, we evaluate the contribution of solar wind to the plasma density on these virtual planes.

B. Contribution from solar wind plasma

The solar wind is primarily a continuous flow of plasma comprising electrons, ions, and neutrals at high temperature. The specification of solar wind plasma has been highlighted in an elegant article by Mann *et al.*;[32] specific data used for the calculations[33] have been given later in the text. For the sake of simplicity in the analysis, the charged particles in the solar wind plasma are considered to exhibit Maxwellian distribution of their energy. Considering the high temperature operating regime and thermal speed of electrons in comparison to the flow speed, this assumption is a reasonable approximation, however, marginally applicable for the heavy ions. With this notion, the momentum distribution of the electrons in the solar wind plasma having momentum between p_e and (p_e+dp_e) can be written as[34,35]

$$d^2n_{se}=n_{so}(2\pi mkT_{se})^{-3/2}(2\pi p_{te})\exp\left[-p_e^2/2mkT_{se}\right]dp_{xe}dp_{te}, \tag{11}$$

where n_{so} refers to the unperturbed peak density of the solar wind plasma at mean operating temperature T_{se}; rest of the parameters have their usual meaning, mentioned before.

The momentum flux normal (x) on any planar surface at positive potential V, over the lunar surface, can be expressed as

$$d^2n_{se}=n_{so}(p_{xe}/m)(1/2\pi mkT_{se})^{3/2}(2\pi p_{te})\times\exp\left[-(p_{xe}^2+p_{te}^2)/2mkT_{se}\right]dp_{xe}dp_{te}=n_{so}(kT_{se}/2\pi m)^{1/2}\exp[-(e_{xe}+e_{te})]de_{xe}de_{te}, \tag{12}$$

where $e_{xe}(=p_{xe}^2/2mkT_{se})$ and $e_{te}(=p_{te}^2/2mkT_{se})$ infer the normal and parallel components of the electron energy normalized with electron temperature. The momentum distribution in terms of normal energy may be obtained by integrating Eq. (12) over $e_{te} \in (0,\infty)$ space and may be expressed as

$$dn_{se} = n_{so}(kT_{se}/2\pi m)^{1/2}\exp(-e_{xe})de_{xe}. \tag{13}$$

It should be noted that the normal energy of the electrons is enhanced by $\upsilon_{we}(=-eV/kT_{se}=\upsilon T_o/T_{se})$ as it approaches the virtual plane at potential V; physically, this may be included either in the distribution function or in the limits of integration. Nonetheless, if one assumes that minimum energy of electrons in the solar wind is zero (no additional potential barrier), then the electrons with $e_{xe}>0$ contribute to the flux over the virtual plane and can be written as

$$n_{se} = \int_0^\infty dn_{se} = n_{so}(kT_{se}/2\pi m)^{1/2}. \tag{14}$$

The electron reaching the planar surface of potential V has net normal energy equivalent to $(e_{xe}-\upsilon_{we})$, and hence, the corresponding electron density at that level can be written as

$$\begin{aligned} n_{we} &= (m/2kT_{se})^{1/2}\int_0^\infty \left[dn_{se}/(e_{xe}-\upsilon_{we})^{1/2}\right] \\ &= (n_{so}/2\pi^{1/2})\exp(-\upsilon_{we})erfc\left[(-\upsilon_{we})^{1/2}\right]. \end{aligned} \tag{15}$$

Similarly, in the case of the ions, the momentum distribution corresponding to the normal flux crossing the virtual plane can be retrieved as

$$dn_{si} = n_{so}(kT_{si}/2\pi m_i)^{1/2}\exp(-e_{xi})de_{xi}, \tag{16}$$

where $e_{xi}(=p_{xi}^2/2mkT_{si})$ refers to the normal energy component of the ion in distribution.

In case the planar surface is at positive potential (V), only those ions, which have energy larger than the surface potential, i.e., $e_{xi}>\upsilon_{wi}(=eV/kT_{si}=\upsilon T_o/T_{si})$, will contribute and hence the net ion flux can be expressed as

$$n_{si} = \int_{\upsilon_{wi}}^\infty dn_{si} = n_{so}(kT_{si}/2\pi m_i)^{1/2}\exp(\upsilon_{wi}). \tag{17}$$

Further, the ion reaching the planar surface of potential V has net normal energy equivalent to $(e_{xi}+\upsilon_{wi})$, and hence, the corresponding ion density at that level at potential V can be written as

$$\begin{aligned} n_{wi} &= (m_i/2kT_{si})^{1/2}\int_{\upsilon_{wi}}^\infty \left[dn_{si}/(e_{xi}+\upsilon_{wi})^{1/2}\right] \\ &= (n_{so}/2)\exp(\upsilon_{wi}). \end{aligned} \tag{18}$$

The two terms derived in Eqs. (15) and (18) infer the density contribution of electrons and ions at any virtual plane, in the formation of the sheath over the lunar surface, respectively. Taking these estimates into account, we next evaluate the sheath structure.

C. Sheath structure

The space evolution of the electric potential in the sheath over the lunar regolith in the steady state may be derived using the Poisson equation where the charge density at any altitude normal to the lunar surface is given by adding all the density contributions from the solar wind plasma and photoemission. Thus potential structure can be written as[21]

$$\left(\frac{d^2V}{dx^2}\right) = 4\pi e n_s \Rightarrow (d^2\upsilon/d\varsigma^2) = -(n_{pe}+n_{we}-n_{wi})/n_{s0}, \tag{19}$$

where $\varsigma=(x/\lambda_d)$, $\lambda_d=(4\pi n_{s0}e^2/kT_o)^{-1/2}$, and $n_{s0}=n_s$ $(\upsilon=\upsilon_o)$.

In the above equation, the term $(n_{pe}+n_{we}-n_{wi})\equiv n_s$ refers to the net population density over the lunar surface characterized by potential υ at an altitude x. Equation (19) can be solved simply by using the appropriate boundary conditions. Multiplying both sides of Eq. (19) by $(2d\upsilon/d\varsigma)$ and using a suitable boundary conditions, *viz.*, $d\upsilon/d\varsigma=0$ and $\upsilon=0$ as $\varsigma\to\infty$, one obtains

$$(d\upsilon/d\varsigma)^2 = -2\int_0^\upsilon \left[(n_{pe}+n_{we}-n_{wi})/n_{co}\right]d\upsilon = [\gamma(\upsilon)]^2. \tag{20}$$

Only the positive square root of $(d\upsilon/d\varsigma)$ is physically tenable. Integrating Eq. (20) with the boundary condition $\upsilon(\varsigma)=\upsilon_o$ as $\varsigma\to 0$, one gets

$$d\varsigma = \left(\frac{d\upsilon}{\gamma(\upsilon)}\right) \Rightarrow \varsigma = \int_{\upsilon_o}^{\upsilon}[1/\gamma(\upsilon)]d\upsilon. \tag{21}$$

From the above analysis, the flux (n), potential (υ), and density (n_s) have been derived as a function of $(\upsilon_o-\upsilon)$ and hence the lunar altitude (ς). The sheath structure in terms of the altitude dependence of density, electric field, and electric potential has been evaluated by solving the set of Eqs. (19)–(21); the results are graphically illustrated in figures in Sec. III.

III. NUMERICAL RESULTS FOR SHEATH FORMATION OVER LUNAR SURFACE

A. Determination of lunar surface potential

In order to illustrate the conceptual basis, it is customary to have notion of the lunar surface potential. As stated before, the photoemission from the regolith surface and the solar wind plasma (comprising electrons/protons) are understood to maintain a plasma environment at the moon (sunlit) surface. The lunar surface usually acquires positive potential under the influence of continuous solar illumination and wind plasma.[21] The steady state potential of the lunar surface may be obtained by balancing the flux associated with photoemission and solar wind plasma; algebraically, this may be presented as

$$n_{ph0}+n_{ic0,s}=n_{ec0,s}, \tag{22}$$

where n_{ph0} refers to the photoemission current to the lunar surface, *i.e.*, $n_{ph}(\upsilon = \upsilon_o)$, while $n_{ec0,s}$ and $n_{ic0,s}$ refer to the electron/ion flux associated with solar wind plasma; the expressions are as follows:[35]

$$n_{ec0,s}(\upsilon_o) = n_{so}(kT_{se}/2\pi m)^{1/2}, \tag{23}$$

$$n_{ic0,s}(\upsilon_o) = n_{so}(kT_{si}/2\pi m_i)^{1/2}\exp(\upsilon_{o,wi}), \tag{24}$$

$$n_{ph0}(\upsilon_o) = \left[\int_{\varepsilon_{\nu 0}}^{\varepsilon_{\nu m}}\left[\frac{\Phi(\upsilon_o+\varsigma_r)}{\Phi(\varsigma_r)}\right]\chi(\varepsilon_\nu)d\Lambda_{cr} + \left[\frac{\Phi(\upsilon_o+\varsigma_{r,L\alpha})}{\Phi(\varsigma_{r,L\alpha})}\right]\chi(\varepsilon_{L\alpha})\Lambda_{L\alpha}\right]. \tag{25}$$

With the help of the above expressions [Eqs. (23)–(25)], Eq. (22) has numerically been solved to obtain steady state potential over the moon surface which has been further used in determining the sheath structure.

B. Computational scheme and data

As a first step, the steady state potential V_o of the lunar surface under the influence of continuous solar radiation and solar wind plasma has been obtained by using *Eq.* (22) with a suitable set of parameters. For this known electric potential V_o (or υ_o), Eq. (20) has been used to evaluate a physically tenable positive value of parameter $\gamma(\upsilon = \upsilon_o)$ corresponding to the moon surface (*i.e.*,$\varsigma = 0$). After knowing the value of $\upsilon(=\upsilon_o)$ and $\gamma(\upsilon = \upsilon_o)$ on the lunar surface ($\varsigma = 0$), Eq. (21) has been solved numerically as an initial value problem to determine the altitude profile of the electric potential (υ) in the lunar sheath; using the altitude profile of potential $\upsilon(\varsigma)$ in the lunar sheath, consequently, the electric field ($\partial_\varsigma\upsilon$) and density ($n_s$) profiles within the sheath have also been evaluated. The dimensionless parameters like ς and υ used in the analysis may be transformed in real units by using the normalization factors λ_d and (kT_o/e).

The typical data[33] for solar wind plasma, *i.e.*, $n_{es} \approx n_{is} \approx 8.7\,\mathrm{cm}^{-3}$ and $T_{es} \approx 2T_{is} \approx 1.4 \times 10^5\,\mathrm{K}$, have been used to determine the potential of the sunlit surface of the moon. Although we are using typical solar wind plasma parameters for the illustration, it should be pointed out that the solar eruptions causing wind plasma are unpredictable and may vary significantly. As per the SPIS (Spacecraft Plasma Interaction Software) manual,[36] the solar wind plasma density may go up to $\sim 23\,\mathrm{cm}^{-3}$ in reference to the NASA worst case. The sun is considered as a black body object radiating at temperature $T_s = 5800\,\mathrm{K}$; a white light solar spectrum ranging up to extreme UV radiation ($0 < \varepsilon_\nu < \varepsilon_{L\alpha}$) and dominant Lyman α radiation (with photon flux $\sim 3 \times 10^{11}/\mathrm{cm}^2\,\mathrm{s}$ and wavelength $\lambda = 121.57\,\mathrm{nm}$) has been considered as the source of electrons from the lunar surface and levitating dust particles. Considering the region across a subpolar point and limb, Grobman and Blank[37] predict a plausible range of the regolith work function in the range of 4 V to 6 V; for the calculation purpose following a recent investigation,[15] the work function of the moon's surface (ϕ_r) is taken to be 6.0 eV. The photoemission rate is assisted with Draine's formulation[31] in accounting for the spectral dependence of the photo-efficiency; χ_0 may take values[38,39] in the range of 0.1–0.5. Another important parameter is the temperature of the lunar sunlit surface which may be evaluated by equating the solar radiation absorbed by the surface to the power lost by thermal radiation and emission cooling. Following the essence of the Diviner Lunar Radiometer Experiment[40] onboard the Lunar Reconnaissance Orbiter (LRO), a consistent value of lunar surface temperature, i.e., $T_o = 400\,\mathrm{K}$, has been taken for computations. The standard set of parameters taken for computation is as follows: $\phi_r = 6.0\,\mathrm{eV}$, $T_o = 400\,\mathrm{K}$, $\chi_0 = 0.5$ (*lunar surface*), $n_{es} \approx n_{is} \approx 8.7/cc$, $T_{es} \approx 1.4 \times 10^5\,\mathrm{K}$, and $T_{is} \approx 7 \times 10^4\,\mathrm{K}$ (*solar wind*). The effect of various parameters on the sheath structure (*viz.*, electric potential/field and density) around the lunar surface has been investigated by varying one and keeping others the same.

C. Results and discussion

The inclusion of solar wind in the analysis might aid the particle (electron/ion) flux and density to the lunar surface (and sheath) in addition to the photoemission induced electron cloud; intuitively in this case, decay in the lunar surface potential and smaller sheath is anticipated. On the other hand, due to the large effective barrier (i.e., work function plus positive potential) for photoemission from the lunar regolith, the continuous solar spectrum marginally contributes to the EUV regime with respect to dominant Lyman-α photons; however, the analysis and calculations take both the contributions into account. As a first step, we evaluate the physical parameters (potential, electric field, and density) on the lunar surface. The dependence of steady state potential of the sunlit lunar surface on the electron (ion) density associated with the solar wind plasma for varying values of photoelectric efficiency (χ_0) is illustrated in Fig. 1(a); for the evaluation of surface potential, Eq. (22) is used. It is noticed that depending on solar wind flux (n_{so}) and photoelectric yield (χ_0) of the material, the lunar surface acquires a positive potential in the range $V_0 \approx (3.5 - 4.5)$ V. The decrease in the lunar surface potential with increasing n_{so} is primarily a consequence of increasing electron accretion flux. The increase in surface potential with the photoelectric yield may be understood in terms of increasing charging current due to photoemission of the electrons from the lunar surface. The subsequent electric field (E_o) and effective population density (n_{s0}) on the lunar surface (i.e., $x = 0$) are illustrated in Figs. 1(b) and 1(c), respectively; the population density is a contribution from the photoemission flux in the steady state (Fig. 1(a), positive potential), while the electric field is in conformance with the Poisson equation [i.e., Eq. (20)] as $(d\upsilon/d\varsigma)_{\varsigma\to 0}$. Using these parameters as initial conditions in solving the Poisson equation for the lunar sheath [Eq. (21)], the characteristic sheath features have been evaluated.

The altitude profile of the electric potential, electric field, and population density over the lunar surface is illustrated in Fig. 2 for different values of n_{so}. The sheath potential is noticed to span over an altitude of $\sim 100\,\mathrm{cm}$ in the absence of solar wind, while its width gradually decays with increasing wind plasma density; for instance, the sheath reduces to $\sim 70\,\mathrm{cm}$ for $n_{so} \sim 8.7\,\mathrm{cm}^{-3}$. This behaviour may be attributed to the contribution of solar wind flux in

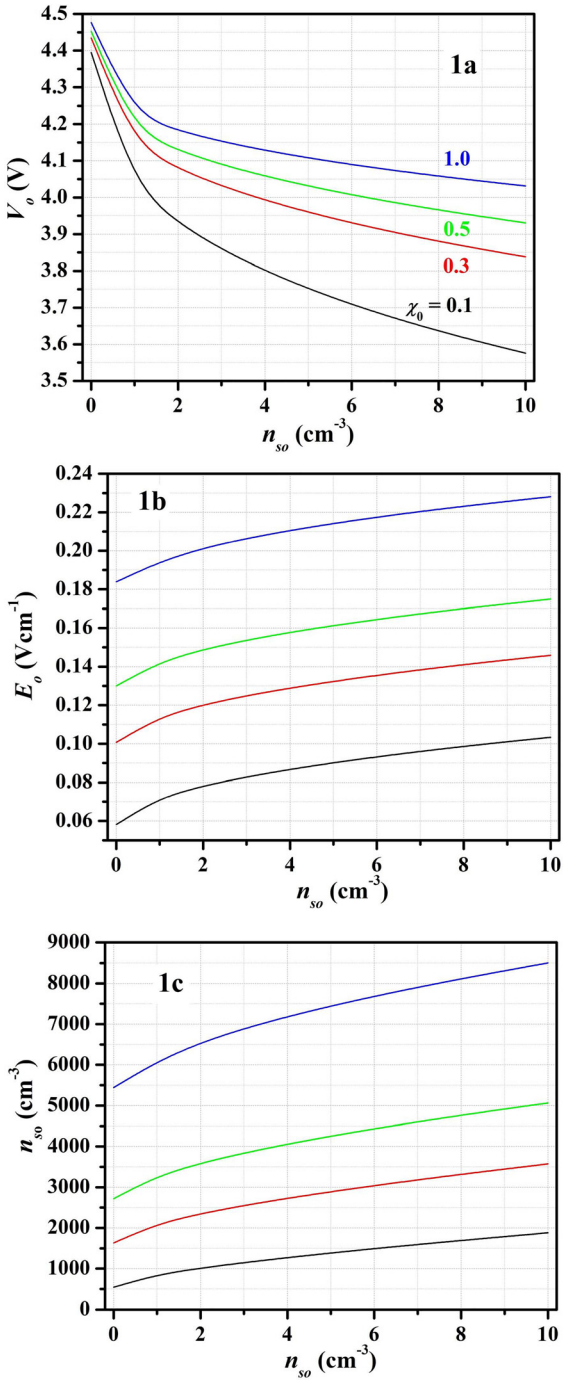

FIG. 1. Dependence of (1*a*) potential (V_o), (1*b*) electric field strength (E_o), and (1*c*) population density (n_{s0}) on the lunar surface ($x = 0$) as a function of solar wind plasma density (n_{so}); the computations correspond to parameters stated in text, while the colour labels refer to different values of χ_0.

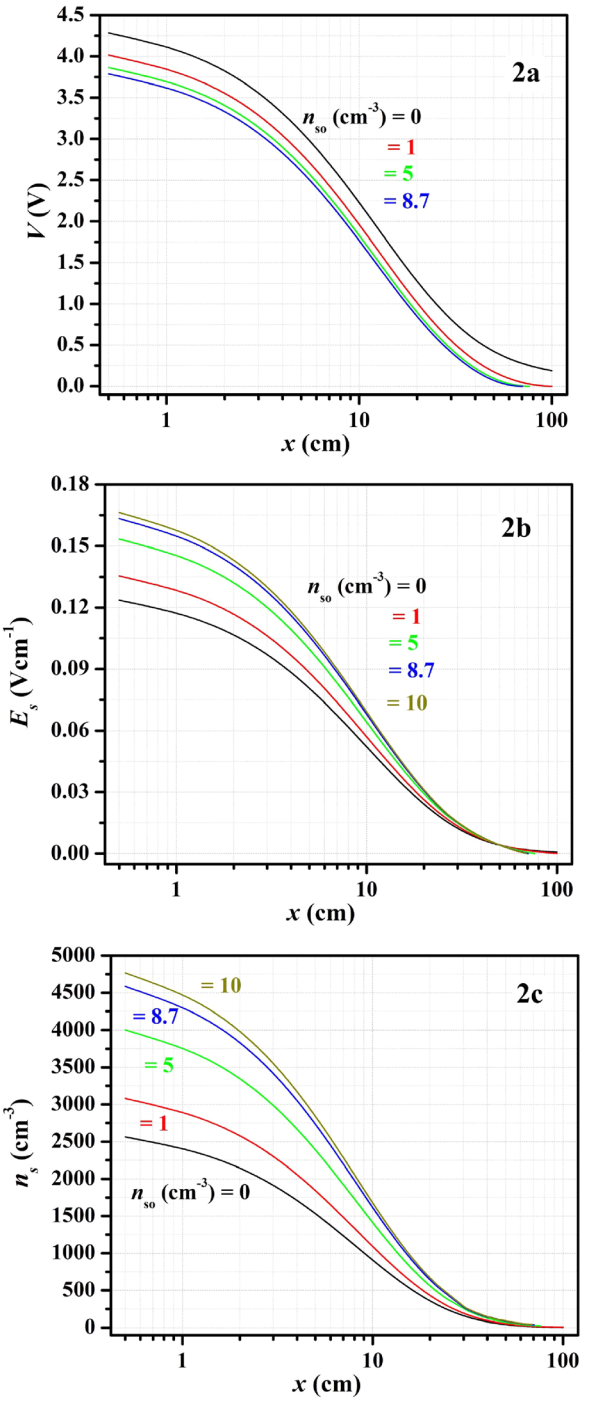

FIG. 2. The altitude profile of (2*a*) sheath potential (V), (2*b*) electric field strength (E_s), and (2*c*) electron population density (n_s) over the lunar surface; computations correspond to the parameters stated in text and the colour labels in figure refer to different values of n_{so}.

determining the lunar surface potential and increase in effective population density. It is also noticed that the electric potential falls steeply for low values of x and then drops slowly with increasing x. The electric field profile which is primarily the derivative of the potential profile is depicted in Fig. 2(b). It is noticed that as the potential gradient becomes smaller for large x [Fig. 2(a)], the field strength (E_s) changes its trend with respect to wind plasma density (around $x \sim 45$ cm) and terminates (i.e., becomes zero) at smaller altitude for large n_{so}. The subsequent density (n_s) corresponding to the potential structure [Fig. 2(a)] is displayed in Fig. 2(c) and is a consequence of reduced incoming/outgoing electron flux with sheath potential V. From this set of calculations, the solar wind plasma is shown to influence the lunar surface features and hence the sheath formation which ultimately reduces the sheath span. After knowing the potential/field structure in the lunar sheath, we next examine the levitation of fine dust particles in the sheath region.

IV. DUST PARTICLE LEVITATION IN LUNAR SHEATH

The sheath structure over the lunar surface is characterized by the altitude profile of the electric field, originated through the positively charged lunar surface, as described in Sec. III. This electric field may support the levitation of positively charged fine particulates in the sheath due to the balance of gravity over the moon surface with the electrostatic force. In the literature,[15] the lunar dust is characterized by the work function smaller than the regolith ($\phi_d \sim 4\,\text{eV}$) and may acquire finite positive potential (V_s) on account of the dominant photoemission process. The equilibrium condition for the dust levitation in the lunar sheath can be expressed as[21]

$$qV + m_d g_m x = qV_o \Rightarrow m_d g_m = qE, \tag{26}$$

where $q\ (= aV_s)$ is the charge on the spherical dust particle of radius a, and $m_d (= 4\pi\rho_d a^3/3)$ and ρ_d refer to the mass and density of the dust particle, respectively, while $g_m = (g_e/6) \approx 163.5 cm/s^2$ is the gravitational acceleration over the moon surface. Equation (26) can be rewritten as

$$a = \left[(3/4\pi)(kT_o/e)^2/\rho_d g_m\right]^{1/2} \upsilon_s^{1/2}(\upsilon_o - \upsilon)^{1/2} x^{-1/2} = a_0(x). \tag{27}$$

Further, for $a < a_0$, the particles move upwards, while for $a > a_0$, they move downwards until they attain an equilibrium position. In order to analyze the levitation, one needs to evaluate the charge (potential) on the dust particles which is eventually the consequence of dynamic equilibrium between the accretion of sheath electron and solar wind plasma along with photoemission flux over the dust particle surface. The flux balance over the spherical dust particles can be expressed as

$$N_{ph}(\upsilon_s - \upsilon) + N_{ic,s}(\upsilon_s - \upsilon) = N_{ec}(\upsilon_s - \upsilon) + N_{ec,s}(\upsilon_s - \upsilon), \tag{28}$$

where N_{ph} refers to the rate of photoelectron emission from the spherical surface at an electric potential $(V_s - V)$ with respect to the surrounding layer at electric potential V, and N_{ec} corresponds to the accretion of the sheath electrons over the spherical surface, while $N_{ec.s}$ ($N_{ic.s}$) corresponds to the accretion current associated with solar wind electrons (ions). Next, we evaluate/define the constituent fluxes.

A. Photoemission flux

The photoemission flux from the levitated spherical dust particles operating at finite temperature (T_d) under the influence of the continuous solar radiation can be written as[35]

$$N_{ph}(\upsilon_s - \upsilon) = \pi a^2 \left[\int_{\varepsilon_{\nu 0}}^{\varepsilon_{\nu m}} \left[\frac{-(\upsilon_{sd} - \upsilon_d) ln\left[1 + \exp(\varsigma_d + \upsilon_{sd} - \upsilon_d)\right] + \Phi(\varsigma_d + \upsilon_{sd} - \upsilon_d)}{\Phi(\varsigma_d)}\right] \chi_d(\varepsilon_\nu) d\Lambda_{cr} + \left[\frac{-(\upsilon_{sd} - \upsilon_d) ln\left[1 + \exp(\varsigma_{d,L\alpha} + \upsilon_{sd} - \upsilon_d)\right] + \Phi(\varsigma_{d,L\alpha} + \upsilon_{sd} - \upsilon_d)}{\Phi(\varsigma_{d,L\alpha})}\right] \chi_d(\varepsilon_{L\alpha}) \Lambda_{L\alpha}\right], \tag{29}$$

where $\varsigma_d = (\varepsilon_\nu - \varphi_d)(T_o/T_d)$, $\varsigma_{d,L\alpha} = \varsigma_d(\varepsilon_\nu = \varepsilon_{L\alpha})$, $\upsilon_{sd} = \upsilon_s(T_o/T_d)$, $\upsilon_d = \upsilon(T_o/T_d)$, $\varphi_d = (e\phi_d/kT_d)$, and χ_d refers to the photoelectric yield of the dust material.

B. Accretion current due to sheath electrons

The sheath electrons contribute to the electron flux accretion over the levitating dust particles. Under the notion of steady state equilibrium of the lunar sheath (comprising electrons, dust particles, and moon surface) and illustration of conceptual basis, as a simplification, the sheath electrons are taken to be at the same temperature equivalent to the lunar surface/dust particles. Considering the levitated dust particles to be at positive potential (V_s), the effective collision cross section of the accreting electrons can be put in the form[35]

$$\sigma(\varepsilon_x, \varepsilon_t) = \pi a^2 [1 - (\upsilon_s - \upsilon)/(\varepsilon_x + \varepsilon_t)]. \tag{30}$$

Using the momentum distribution of electrons in the lunar sheath as half Fermi-Dirac statistics,[31] the rate of electron accretion on the spherical particle due to outward flux may be written as[21]

$$N_{eco} = \frac{1}{2}\int_0^\infty \int_0^\infty \sigma(\varepsilon_x, \varepsilon_t) d^2 n_{ph} = \left(\frac{\pi a^2}{2}\right)\left[\int_{\varepsilon_{\nu 0}}^{\varepsilon_{\nu m}} \left(\frac{\chi(\varepsilon_\nu)}{\Phi(\varsigma_r)}\right)\left(\int_0^\infty \varepsilon\left(1 - \frac{\upsilon_s - \upsilon}{\varepsilon}\right) \times F_D(\varepsilon - \varsigma_r - \upsilon_o + \upsilon) d\varepsilon\right) d\Lambda_{cr} + \left(\frac{\chi(\varepsilon_{L\alpha})}{\Phi(\varsigma_{r,L\alpha})}\right)\Lambda_{L\alpha} \times \int_0^\infty \varepsilon\left(1 - \frac{\upsilon_s - \upsilon}{\varepsilon}\right) F_D(\varepsilon - \varsigma_{r,L\alpha} - \upsilon_o + \upsilon) d\varepsilon\right]. \tag{31}$$

Following the approach similar to Sec. II A, the electrons having radial energy less than dust potential $\varepsilon_x < (-\upsilon)$ will return back to the particle, and hence, the rate of electron accretion on account of the inward flux can be expressed as

$$N_{eci} = N_{eco} - \left(\frac{\pi a^2}{2}\right)\left[\int_{\varepsilon_{\nu 0}}^{\varepsilon_{\nu m}} \left(\frac{\chi(\varepsilon_\nu)}{\Phi(\varsigma_r)}\right)\left(\int_0^\infty \varepsilon\left(1 - \frac{\upsilon_s - \upsilon}{\varepsilon - \upsilon}\right) \times F_D(\varepsilon - \varsigma_r - \upsilon_o) d\varepsilon\right) d\Lambda_{cr} - \left(\frac{\chi(\varepsilon_{L\alpha})}{\Phi(\varsigma_{r,L\alpha})}\right)\Lambda_{L\alpha} \times \int_0^\infty \varepsilon\left(1 - \frac{\upsilon_s - \upsilon}{\varepsilon - \upsilon}\right) F_D(\varepsilon - \varsigma_{r,L\alpha} - \upsilon_o) d\varepsilon\right]. \tag{32}$$

The net accretion current associated with sheath electrons on a spherical grain at a layer characterized by an electric potential (V) can be expressed as

$$N_{ec}(\upsilon_s - \upsilon) = N_{eco} + N_{eci}. \tag{33}$$

It is evident from the above derived expressions for accretion current of the sheath electrons that it significantly depends on the nature of electron energy distribution in the sheath.[21]

C. Accretion flux associated with solar wind plasma

As discussed in an earlier section (Sec. II B), the solar wind has been approximated by plasma comprising electrons and ions at high temperature exhibiting Maxwellian statistics. With this simplification, the collision cross section of electrons and ions accreting over the positively charged dust particle may be expressed as[35]

$$\sigma_e(e_{xe}, e_{te}) = \pi a^2\left[1 - (\upsilon_{s,we} - \upsilon_{we})/(e_{xe} + e_{te})\right], \tag{34a}$$

$$\sigma_i(e_{xi}, e_{ti}) = \pi a^2\left[1 + (\upsilon_{s,wi} - \upsilon_{wi})/(e_{xi} + e_{ti})\right], \tag{34b}$$

where $\upsilon_{s,we}(=\upsilon_s T_o/T_{se})$, $\upsilon_{s,wi}(=\upsilon_s T_o/T_{si})$, and $e_{e,i} = (e_{xe,xi} + e_{te,ti})$.

Following the orbital motion limited (OML) based approach[35] for determining the accretion current of the electrons/ions over positively charged dust particles levitating at sheath layer with potential V, the electron and ion accretion current associated with the solar wind plasma may be expressed as[35]

$$\begin{aligned} N_{ec,s}(\upsilon_s - \upsilon) &= n_{so}(kT_{se}/2\pi m)^{1/2}\pi a^2 \\ &\quad \times \int_0^\infty e_e\left(1 - \frac{(\upsilon_{s,we} - \upsilon_{we})}{e_e}\right)\exp(-e_e)de_e \\ &= n_{so}(kT_{se}/2\pi m)^{1/2}\pi a^2\left[1 - (\upsilon_{s,we} - \upsilon_{we})\right], \end{aligned} \tag{35}$$

$$\begin{aligned} N_{ic,s}(\upsilon_s - \upsilon) &= n_{so}(kT_{si}/2\pi m_i)^{1/2}\pi a^2 \\ &\quad \times \int_0^\infty e_i\left(1 + \frac{(\upsilon_{s,wi} - \upsilon_{wi})}{e_i - (\upsilon_{s,wi} - \upsilon_{wi})}\right) \\ &\quad \times \exp\left[-(e_i - \upsilon_{s,wi} + \upsilon_{wi})\right]de_i \\ &= n_{so}(kT_{si}/2\pi m_i)^{1/2}\pi a^2 \exp(\upsilon_{s,wi} - \upsilon_{wi}). \end{aligned} \tag{36}$$

With the help of expressions derived herein, Eqs. (27) and (28) may numerically be solved to determine particle charging and optimum particle size within the lunar sheath. It should be mentioned here that the role of photoemission from particles has been ignored in determining the sheath structure over the lunar surface.

V. NUMERICAL RESULTS FOR FINE PARTICLE LEVITATION IN THE SHEATH

Taking forward the knowledge of the photoelectron sheath, i.e., altitude profile of the electric potential, electric field, and population density (Fig. 2), we use $\upsilon(\varsigma)$ relation and expressions [Eqs. (29), (33), (35), and (36)] to solve Eq. (28) numerically and evaluate the steady state mean surface potential (υ_s) over the levitating dust grains in the lunar sheath. In describing the charging of fine dust particles in the sheath region, uniform potential theory is applied where the photoemission and accretion (of sheath electrons/solar wind plasma) are considered as dominant charging mechanisms. For the sake of simplicity in analysis, Mie scattering[41] of the radiation from levitating fine particles and size dependence of the photoelectric yield[21] have been ignored, which is pertinent for the particles larger than 200 nm. The theory presented herein is also limited by the fact that the dust particle number density is such that the photoelectron sheath structure remains unaffected. The uniform potential approach yields an important consequence that the steady state potential is independent of the particle size,[42] and hence, charge on the surface increases linearly with the radius ($z_s \propto a$). Manifesting the known value of particle charge (via potential V_s) on levitating grains with the electric field altitude profile in the lunar sheath (E_s), one may obtain the optimum particle size as a function of lunar surface altitude using Eq. (27). For the computations, the same set of solar wind and photon flux data as in Sec. III B has been used. Draine's formulation[28] has been used to describe the spectral dependence of the photoelectric efficiency of the levitating fine particles, while considering the recent analysis,[30] their work function (ϕ_d) and density (ρ_d) are taken to be 4.0 eV and ~3.0 g/cm^3, respectively. The parameters for dust particulates used in these calculations, in addition to solar radiation/wind, are as follows: $\phi_d = 4.0\,\text{eV}$, $T_d = 400\,\text{K}$, $\chi_0 = 0.5$, and $\rho_d = 3g/cc$. Next, we discuss the dust particle charging and their levitation in the sheath for the standard case.

In contrast to the lunar regolith, due to the low work function of the particulates, the charging is significantly influenced by the continuous solar radiation spectrum ($h\nu > \phi_d$). Further, due to the presence of solar wind plasma, the particle potential (charge) is anticipated to decrease on account of electron accretion flux. The dependence of the steady state dust potential (V_s) on the surface altitude (x) in the presence (red) and absence (black) of the solar wind is illustrated in Fig. 3(a). The decaying nature of the dust surface potential may be attributed to the potential profile in the photoelectron sheath [Fig. 2(a)]. The reduction in positive potential in the presence of solar wind may be understood in terms of enhanced electron flux over dust particles associated with wind plasma. After knowing dust potential, the altitude dependence of the maximum possible radius of the dust particle which can levitate in the presence of electrostatic sheath field is illustrated in Fig. 3(b); this nature is in conformance with the altitude profile of the sheath electric field [E_s, Fig. 2(b)]. For this particular set of parameters, it is noticed that the levitation terminates around ~70 cm in the presence of solar wind while it continues up to ~100 cm when the effect of solar wind is ignored. In addition, the optimum particle size is little higher at lower altitude ($x < 40$ cm) when the solar wind is considered; however, in consistency with the sheath electric field profile [Fig. 2(b)], its value drops rapidly at higher lunar altitudes ($x > 45$ cm). At lower altitudes, the photoelectron sheath may hold submicron size particles; for instance, 500 and 200 nm particles are predicted to float up to ~10 cm and ~32 cm, respectively, in the photoelectron sheath.

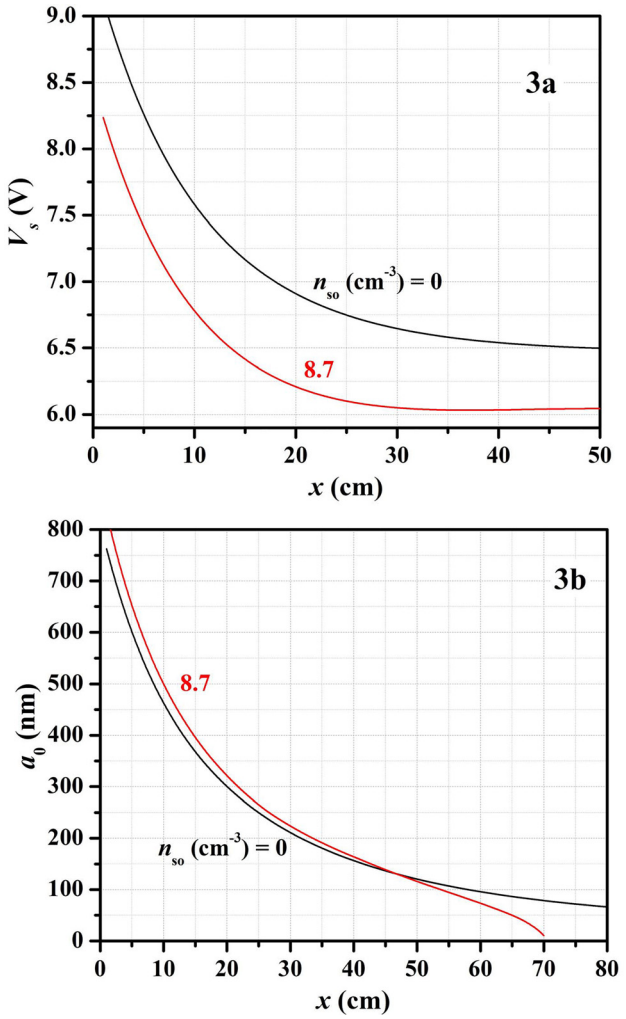

FIG. 3. The altitude profile of (3*a*) the dust surface potential (V_s) and (3*b*) optimum particle size within lunar photoelectron sheath; computations correspond to the parameters stated in text and the colour labels in figure refer to different values of n_{so}.

VI. SUMMARY AND CONCLUSIONS

In summary, a self-consistent analytical model describing the photoelectron sheath structure over the lunar surface has been developed. The formulation includes the continuous solar spectrum, solar flux plasma, and half Fermi-Dirac distribution of photoelectron velocities in evaluating the sheath structure through the Poisson equation; considering the simplified Maxwellian nature of solar wind plasma, the expressions for its contribution to the electron/ion population density has been derived. After a notion of the lunar sheath structure, the levitation of fine dust particles over the moon surface has been examined by taking adequate expressions (derived herein) for anisotropic flux in the photoelectron sheath, solar wind flux, and photoemission over dust particles into account. In deriving the sheath structure and dust levitation phenomena, the steady state potential over the lunar regolith and dust particulates has consistently been determined by balancing the flux of electrons and ions over respective surfaces. As an illustration of the conceptual basis, the altitude profile of the electric potential/electric field and population density in the lunar sheath has been depicted; in particular, the role of solar wind plasma has been identified. The analysis presented herein is of general in nature and is applicable to any other resembling physical scenario in nature and laboratory experiments. The solar wind plasma is noticed to suppress the sheath width and demonstrate high constituent electric field which eventually leads to the levitation of large particles at lower altitudes.

The analysis presents a comprehensive model for the structure of photoelectron sheath and levitation of dust, based on sound physics. As the analysis takes account of few simplifications, it is reasonable to comment on its applicability; here, we discuss the limitations of the present analysis and consequent effects. As a simplification, the electrons (ions) in the solar wind plasma are considered to be of Maxwellian in nature, which eventually should be characterized by shifting Maxwellian distribution of velocity (in particular ions); in such a case, the accretion current[43,44] decreases and the particles are supposed to gain higher positive potential, which may result in higher levitation altitude. The observed solar wind is noted to comprise a variety of electron (and ion) energy population; for instance, in an elegant study,[45] the electrons in high speed solar wind are ascribed to core (low energy) and halo and strahl (high energy) populations. On account of different temperature/population densities of the constituent core and halo/strahl, electrons may characterize different accretion flux over the lunar surface and dust particulates; the inclusion of such distributions might influence the lunar surface potential and hence the sheath structure. Qualitatively, the increase (decrease) in the electron population/temperature in the distribution ultimately leads to the larger (smaller) collection current and reduced (high) surface potential which eventually may cause a smaller (larger) sheath span; similarly, the charge of the levitated dust is also affected and one may anticipate the lower (higher) altitude of levitation. It should also be stated that though the analysis has been performed for simplified Maxwellian statistics of the solar wind plasma constituents, the analytical approach is equally applicable and reiterated for any specified distribution. Further, in the exotic cases (corresponding to extreme solar activities), the solar wind plasma density is reported[46,47] to reach the order of $\sim 100\,\mathrm{cm}^{-3}$. On the basis of present analysis and understanding, under these extreme conditions when solar flux is high, the lunar surface potential and the sheath span are expected to reduce; subsequently, the levitating particle charge may also be anticipated to be small and hence lower altitude of levitation. Another concern is the Mie scattering of radiation from smaller dust particulates[41] ($2\pi a/\lambda < 10$), which might reduce the mean particle charge and hence the optimum size of the dust particles for levitation. As another simplification, the role of levitated particles in the lunar sheath is ignored; the photoemitted electrons from dust may lead to the increase in density population in the sheath which in turn may reduce the sheath expansion. Further uniform surface potential, which is primarily pertinent to conducting substances, is taken in order to avoid the complexity associated with dielectric (non-conducting) materials. In this context, another concern may be the surface inhomogeneity which might lead to an inhomogeneous photoelectron sheath

and hence irregular particle levitation/distribution. Although these aspects limit the applicability of the presented results, the analytical formulation gives a feasible solution (and scaling) of lunar sheath features and puts forward a basis for further advancement. This work may also be of practical significance in designing test experiments in labs for future lunar/space campaigns.

ACKNOWLEDGMENTS

This work was performed under ELI-ALPS Project (No. GINOP-2.3.6-15-2015-00001) which is supported by the European Union and co-financed by the European Regional Development fund.

[1]J. J. Rennilson and D. R. Criswell, Moon **10**, 121 (1974).
[2]H. Zook and J. McCoy, Geophys. Res. Lett. **18**, 2117, https://doi.org/10.1029/91GL02235 (1991).
[3]J. E. Colwell, S. Batiste, M. Horanyi, and S. Store, Rev. Geophys. **45**, 26, https://doi.org/10.1029/2005RG000184 (2007).
[4]D. R. Criswell, "Lunar dust motion," in Proceedings of the Lunar Science Conference (1972), Vol. 3, p. 2671.
[5]D. R. Criswell, "Horizon-glow and the motion of lunar dust," in *Photon and Particle Interactions with Surfaces in Space*, edited by R. J. L. Grard (Reidel, Dordrecht, 1973), p. 545.
[6]J. E. McCoy and D. R. Criswell, in Proceedings of the Lunar Science Conference (1973), Vol. 5, p. 496.
[7]R. L. Guernsey and J. H. M. Fu, J. Geophys. Res. **75**, 3193, https://doi.org/10.1029/JA075i016p03193 (1970).
[8]S. F. Singer and E. H. Walker, Icarus **1**, 112 (1962).
[9]J. E. Colwell, A. S. Amanda Gulbis, M. Horanyi, and S. Robertson, Icarus **175**, 159 (2005).
[10]T. J. Stubbs, R. R. Vondrak, W. M. Farrel, and M. R. Collier, J. Astronautics **28**, 166 (2007).
[11]Z. Sternovsky, P. Chamberlin, M. Horanyi, S. Robertson, and X. Wang, J. Geophys. Res. **113**, A10104, https://doi.org/10.1029/2008JA013487 (2008).
[12]J. S. Halekas, G. T. Delory, R. P. Lin, T. J. Stubbs, and W. M. Farrell, J. Geophys. Res. **113**, A09102, https://doi.org/10.1029/2008JA013194 (2008).
[13]A. Poppe and M. Horanyi, J. Geophys. Res. **115**, A08106, https://doi.org/10.1029/2010JA015286 (2010).
[14]A. P. Goulob, G. G. Dolrikov, and A. V. Zakharov, JETP Lett. **95**, 182 (2012).
[15]S. I. Popel, S. I. Keprni, A. P. Golub, G. G. Dolmikov, A. V. Zakhorov, L. M. Zebenyi, and Y. N. Izvekov, Sol. Syst. Res. **47**, 419 (2013).
[16]J. S. Halekas, A. Poppe, G. T. Delory, W. M. Farrell, and M. Horanyi, Earth Planets Space **64**, 73 (2012).
[17]A. R. Poppe, J. S. Halekas, G. T. Delory, W. M. Farrell, V. Angelopoulos, J. P. McFadden, J. W. Bonnell, and R. E. Ergun, Geophys. Res. Lett. **39**, L01102 (2012).
[18]T. Nitter, O. Havnes, and F. Melandsø, J. Geophys. Res. **103**, 6605, https://doi.org/10.1029/97JA03523 (1998).
[19]R. H. Fowler, Phys. Rev. **38**, 45 (1931).
[20]W. W. Roehr, Phys. Rev. **44**, 866 (1933).
[21]M. S. Sodha and S. K. Mishra, Phys. Plasmas **21**, 093704 (2014).
[22]S. Misra, S. K. Mishra, and M. S. Sodha, Phys. Plasmas **22**, 043705 (2015).
[23]M. S. Sodha and S. K. Mishra, Phys. Plasmas **23**, 022115 (2016).
[24]A. Dove, M. Horanyi, X. Wang, M. Piquette, A. R. Poppe, and S. Robertson, Phys. Plasmas **19**, 043502 (2012).
[25]A. R. Poppe, M. Piquette, A. Likhanskii, and M. Horanyi, ICARUS **221**, 135 (2012).
[26]E. A. Lisin, V. P. Tarakanov, S. I. Popel, and O. F. Petov, J. Phys.: Conf. Ser. **653**, 012139 (2015).
[27]S. Misra and S. K. Mishra, MNRAS **432**, 2985 (2013).
[28]S. J. Bauer, *Physics of Planetary Ionosphere* (Springer Verlag, New York, 1973).
[29]M. S. Sodha, S. K. Mishra, and S. Misra, Phys. Plasmas **16**, 123701 (2009).
[30]F. Seitz, *Modern Theory of Solids* (McGraw-Hill Book Co, New York, 1940).
[31]B. T. Draine, Astrophys. J. Suppl. Ser. **36**, 595 (1978).
[32]I. Mann, A. Pellinen-Wannberg, E. Murad, O. Popova, N. Meyer-Vernet, M. Rosenberg, T. Mukai, A. Czechowski, S. Mukai, J. Safrankova, and Z. Nemecek, Space Sci. Rev. **161**, 1 (2011).
[33]S. I. Popel, L. M. Zebenyi, and B. Atamaniuk, Plasma Phys. Rep. **42**, 555 (2016).
[34]R. H. Fowler, *Statistical Mechanics: The Theory of the Properties of Matter in Equilibrium* (Cambridge University Press, London, 1955).
[35]M. S. Sodha, *Kinetics of Complex Plasmas* (Springer, New Delhi, 2014).
[36]See http://dev.spis.org/projects/spine/home/ for SPIS simulation manual.
[37]W. D. Grobman and J. L. Blank, J. Geophys. Res. **74**, 3943, https://doi.org/10.1029/JA074i016p03943 (1969).
[38]M. A. Fenner, J. W. Freeman, and H. K. Hills, in Proceedings of the Fourth Lunar Science Conference (1973), Vol. 03, p. 2877.
[39]A. A. Sickafoose, J. E. Colwell, M. Horanyi, and S. Robertson, J. Geophys. Res. **106**, 8343, https://doi.org/10.1029/2000JA000364 (2001).
[40]J.-P. Williams, D. A. Paige, B. T. Greenhagen, and E. Sefton-Nash, Icarus **283**, 300 (2017).
[41]M. S. Sodha, S. K. Mishra, and S. Misra, J. Appl. Phys. **109**, 013303 (2011).
[42]M. S. Sodha, S. Misra, and S. K. Mishra, Phys. Plasmas **17**, 113705 (2010).
[43]V. E. Fortov, A. V. Ivlev, S. A. Khrapak, A. G. Khrapak, and G. E. Morfill, Phys. Rep. **421**, 01 (2005).
[44]S. K. Mishra, S. Misra, and M. S. Sodha, Phys. Plasmas **18**, 103708 (2011).
[45]V. Pierrard, M. Maksimovic, and J. Lemaire, Astrophys. Space Sci. **277**, 195 (2001).
[46]J. T. Gosling, E. Hildner, J. R. Asbridge, S. J. Bame, and W. C. Feldman, J. Geophys. Res. **82**, 5005, https://doi.org/10.1029/JA082i032p05005 (1977).
[47]S. Shodhan, N. U. Crooker, R. J. Fitzenreiter, R. P. Lepping, and J. T. Steinberg, AIP Conf. Proc. **471**, 601 (1999).